Research Article Vol. 3, No. 1 / 15 January 2020 / OSA Continuum 132

Thermally-induced optical modulation in a vanadium dioxide-on-silicon waveguide

VADIVUKKARASI JEYASELVAN,[1] ANAND PAL,[2,3] P. S. ANIL KUMAR,[2] AND SHANKAR KUMAR SELVARAJA[1,*]

[1]Centre for Nano Science and Engineering, Indian Institute of Science, Bangalore, India
[2]Department of Physics, Indian Institute of Science, Bangalore, India
[3]Department of Physics, Manipal Institute of Technology, Manipal Academy of Higher Education, Manipal 576104, Karnataka, India
[*]shankarks@iisc.ac.in

Abstract: In this paper, we report phase-pure vanadium dioxide (VO_2) deposition on silicon-on-insulator and demonstrate switching/modulation exploiting the phase-change property. We present electrical and optical properties of VO_2 during phase transition. Exploiting the phase change property, optical modulation is achieved by thermally tuning the VO_2 phase using a lateral micro-heater beside the waveguide. We achieve an optical modulation extinction of 25 dB and a low insertion loss of 1.4 dB using a ring resonator with a VO_2 patch. We also demonstrate the switching performance of a symmetric Mach-Zehnder interferometer and present a detailed discussion on the optimal operating point to achieve maximum modulation, higher speed, and lower insertion loss.

1. Introduction

Recently, phase-change materials (PCMs) have shown great promise for applications in integrated optics platform [1,2] due to their broadband operation and CMOS compatibility. Of all the PCMs, VO_2 has gained particular attention because of its transition from insulating, optically transmissive monoclinic phase to metallic and optically opaque tetragonal rutile phase, at very near to the room temperature (68 °C). The phase transition in VO_2 can be achieved by applying thermal [3,4], optical [5–8] or electrical stimuli [9–11]. These two phases have high contrast in the electrical resistivity (> 3 order change) and optical constants (Δn and $\Delta k > 1$ order change) in the telecommunication wavelength region [12,13]. The refractive index of VO_2 changes from $3.21 + i0.17$ to $2.15 + i2.79$ (at 1550 nm) between the dielectric and metallic phase, respectively [14]. The larger change in refractive index is exploited in the implementation of energy-efficient devices with smaller footprint, such as optical modulators [14–18] and photonic memories [19–22]. The Oxygen stoichiometry plays a crucial role in governing the transport and optical properties of VO_2 [23,24]. Oxygen vacancies can enhance the conductivity and deteriorate the switching properties of VO_2. So, the phase purity and quality of the thin film are very crucial to incorporate VO_2 in these devices. Due to the multiple oxidation states of vanadium, optimization of the deposition and fabrication condition of VO_2 modulator are very critical and challenging [25]. To overcome these problems various techniques such as sputtering [11], chemical vapor deposition [26], pulsed-laser deposition [27], nebulized spray pyrolysis [28] has been reported.

Recently there have been many demonstrations on optic modulation using VO_2-Si waveguide across the metal-insulator transition of VO_2. Briggs et al., achieved extinction of 6.5 dB and an insertion loss of 2 dB using 2 μm long device [14]. An interesting geometry using embedded PCM along the waveguide was demonstrated with an extinction of 10 dB [15]. However, the insertion loss was 6 dB, which is on the high-side. Whereas, Joushaghani et al. enhanced the extinction to 12 dB with a higher insertion loss of 5 dB with an active length of 1 μm [18]. The authors also demonstrated a bandwidth of 1.3 MHz limited by the thermal dissipation. To exploit

#382861 https://doi.org/10.1364/OSAC.382861
Journal © 2020 Received 8 Nov 2019; accepted 17 Dec 2019; published 15 Jan 2020

OSA CONTINUUM

VO_2, it is essential that the three performance parameters; extinction, insertion loss and speed, are optimised through the material and device design.

In this work, we demonstrate an absorption type optical modulator on silicon-on-insulator (SOI) platform by thermally tuning the refractive index of VO_2. Pulsed-laser deposition (PLD) technique is used to grow the phase pure VO_2 thin film on SOI substrate. The phase purity and the evolution of insulating to the metallic phase of as grown VO_2 thin film were characterized using X-Ray Diffraction (XRD) and Raman spectroscopy. We also perform temperature-dependent electrical resistance and ellipsometry measurements to characterize the change in electrical resistance and optical constants of the material across the phase transition. Using VO_2-on-silicon, we demonstrate phase transition using micro-heater and substrate heater. We achieved a maximum optical transmission extinction of ~25 dB in both local heating and global heating with a low insertion loss of 1.4 dB. We also show that the refractive index change measured is ≈1.2 that agrees with spectroscopic ellipsometry on a thin film. We also analyzed the switching performance of the device and optimized the operation condition for the VO_2-based Mach-Zehnder modulators.

2. Material characterization

Phase pure VO_2 is deposited on SOI using V_2O_5 as the target. The details of thin-film depositions protocols were reported earlier in [27]. The phase purity and insulator-metal transition (IMT)/metal-insulator transition (MIT) of the fabricated VO_2 device are characterized using XRD, Raman spectrometer, spectroscopic ellipsometer, and temperature-dependent electrical resistivity measurement. XRD patterns of the deposited films are shown in Fig. 1(a). It is evident from Fig. 1(a) that VO_2 film deposited on SOI is in pure monoclinic (insulating) phase. No sign of any parasitic phase has been observed within the XRD limit [29].

The room temperature Raman spectrum of VO_2 films deposited on SOI substrate is shown in Fig. 1(b). All the main peaks of the Raman spectrum are indexed well with Raman active mode of the monoclinic (insulating) phase of VO_2 without any other impurity phase in the system [28]. The observed room temperature Raman spectrum is in full agreement with previous reports in the literature. The peak at 532 cm^{-1} corresponds to substrate peak. It should be noted that the Raman modes slightly shift to the higher frequency (1 cm^{-1}), which can be attributed to the strain induced by the significant lattice mismatch between film and substrate. To check the evolution of the VO_2 phase, we have carried out Raman measurement at various temperature across the metal-insulator transition. The representative temperature-dependent Raman spectra for VO_2 thin film is shown in Fig. 1(c). The two low-frequency peak 194 cm^{-1} (Ag(1)) and 225 cm^{-1} (Ag(2)) are ascribed to the V-ions motion within the V-V chains, and the high-frequency peak 617 cm^{-1} (Ag(7)) corresponds to the V-O vibration mode. All the Raman modes broaden and weaken with increasing temperature until reaching the transition temperature. Above the transition temperature, all the Raman peaks disappear, which indicates the transition of VO_2 thin film from monoclinic M1 phase to rutile phase. The transition temperature obtained by Raman and electrical transport is the same.

The temperature-dependent electrical resistance of the VO_2 layer during heating and cooling are shown in Fig. 2(a). The resistance measurements are performed using a two-point probe method and the resistance of VO_2 thin films changes from 8.3 MΩ (insulating phase) to 7.3 kΩ (metallic phase). As clearly seen from Fig. 2(a), the film shows a three order change in electrical resistance across the transition. A thermal hysteresis behaviour has been observed upon heating and cooling, which is a typical feature of VO_2. The metal-insulator transition temperature (T_{IMT} or T_{MIT}) is obtained from the first derivative of electrical resistivity with respect to temperature, shown in Fig. 2(b). The transition temperature of VO_2 layer during heating and cooling cycle is 82 °C and 70 °C, respectively. The width of thermal hysteresis is around 12 °C. The slightly larger hysteresis is attributed to the polycrystalline nature of the thin film.

OSA CONTINUUM

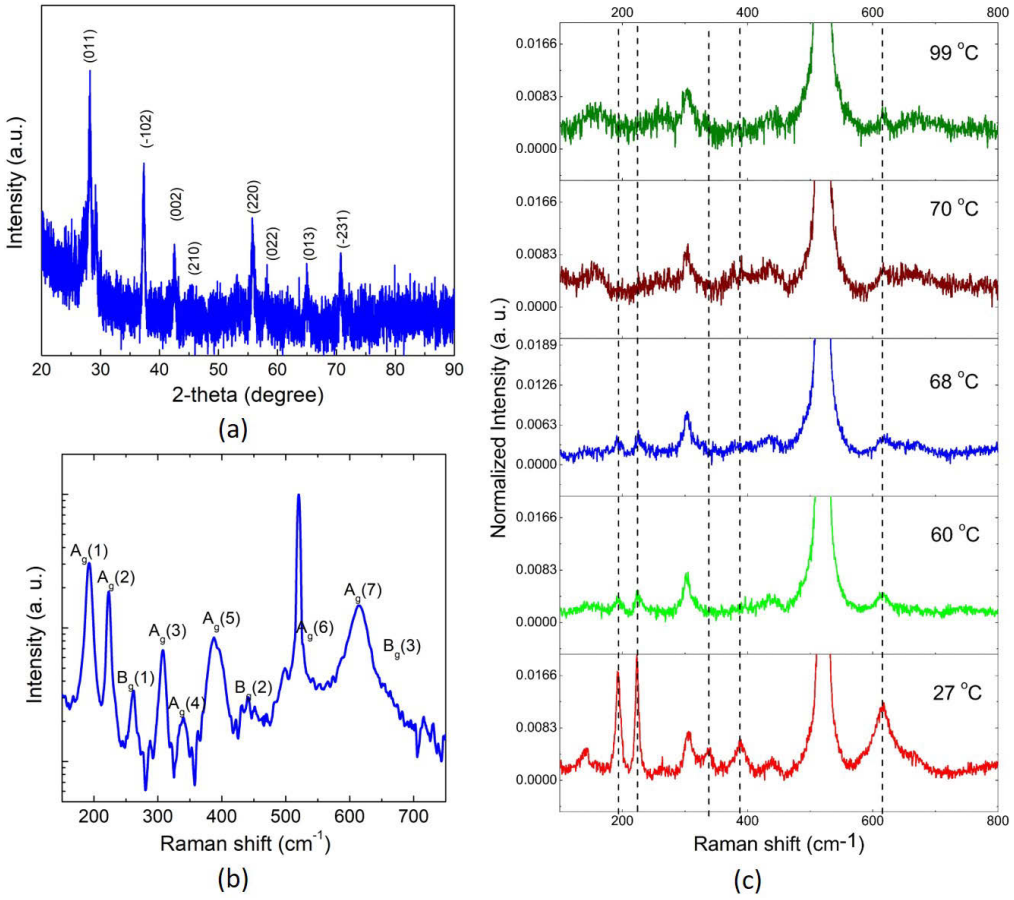

Fig. 1. Material characterization summary of VO_2. (a) XRD pattern of VO_2 thin film on SOI substrate, (b) Raman spectrum of VO_2 at room temperature, and (c) Raman spectrum at various temperature.

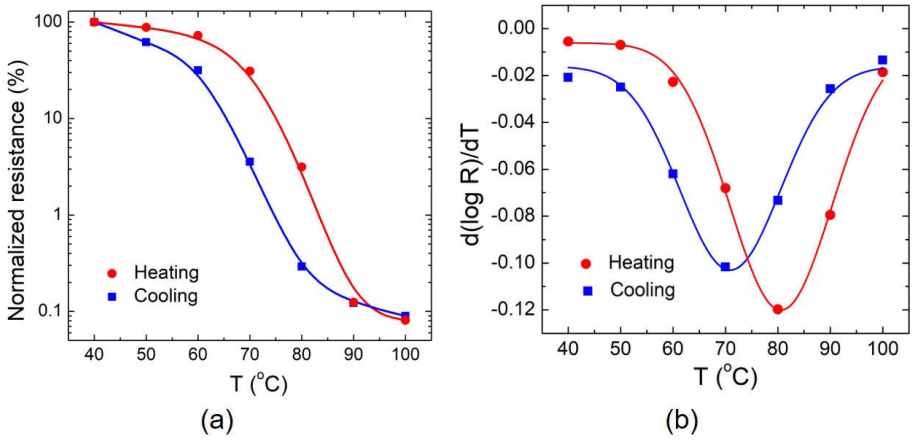

Fig. 2. Summary of electrical characterization of VO_2, (a) Temperature dependent electrical resistance measurement during heating and cooling cycle across the transition of the studied device, (b) First derivative of electrical resistance with respect to temperature during the heating and cooling cycle.

OSA CONTINUUM

The metal-insulator transition in VO_2 is accompanied by a substantial change in the refractive index. The refractive index of the VO_2 layer is measured using spectroscopic ellipsometry (250 to 1000 nm). The measurements are done at various angles (65°-75°) to build a material model to extract the optical constants. Temperature dependent ellipsometer measurement is performed to analyze the optical constant evolution during heating and cooling cycle. In the dielectric phase, the optical constants are fit to a Lorentzian model whereas, in the metallic phase, Drude contribution is also included with Lorentz to model VO_2 absorption spectrum [30]. Figure 3 shows the refractive index (n and k) of a 70 nm thick film on SOI substrate. Refractive index profile exhibits hysteresis of phase transition similar to electrical conductivity. When $T>T_{MIT}$, n reduces and k increases and vice-versa when $T<T_{IMT}$. The change in temperature-dependent optical parameters Δn and Δk at 1000 nm is 1.93 and 0.77, respectively. The thickness for the VO_2 film is verified using step height measurement.

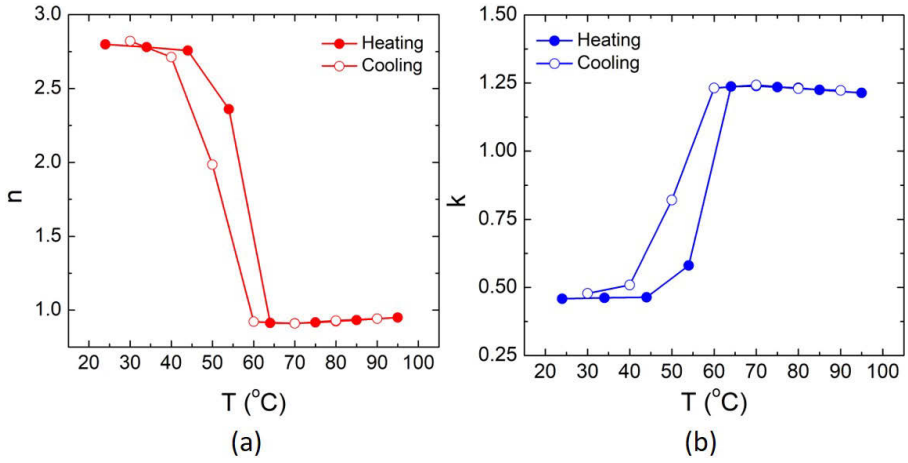

Fig. 3. Temperature dependent refractive index measurement of VO_2 at wavelength of 1000 nm using spectroscopic ellipsometry (a) n and (b) k.

3. Results and discussion

3.1. Design and fabrication overview

The device is fabricated on an SOI substrate with 220 nm thick silicon and 2 μm buried oxide. A planarized shallow etched rib configuration is used to define waveguides, ring resonator, and Mach-Zehnder interferometer.

Figure 4(a-d) shows the fabrication process flow overview. Figure 4(a) shows the cross-section schematic of a planarized rib waveguide [31]. On top of the rib waveguide, a 40 nm thick SiO_2 is deposited using plasma-enhanced chemical vapor deposition process (Fig. 4(b)). Following SiO_2 deposition, a 70 nm thick VO_2 film is deposited using V_2O_5 as PLD target material. A substrate temperature of 580 °C is maintained during deposition at 10 mTorr oxygen pressure [27] (Fig. 4(c)). The sample is then spin-coated with photoresist and patterned using direct laser writer. VO_2 patches on top of the device are etched using reactive ion etching process by a mixture of Ar and Cl gas followed by wet etching using a mixture of perchloric acid and ceric ammonium nitrate to soft-land on SiO_2 (Fig. 4)). Combination of dry etch followed by a wet etch process avoids damage to underlying device. Furthermore, lateral etch of VO_2 due to wet etch process is reduced by this two-step etch. The oxide liner on top of the planarized waveguide also help in protecting the underlying device and also helps in preventing metal diffusion into silicon

OSA CONTINUUM

that could potentially result in higher insertion loss due to absorption in the waveguide. For light in and out-coupling focused grating couplers were used.

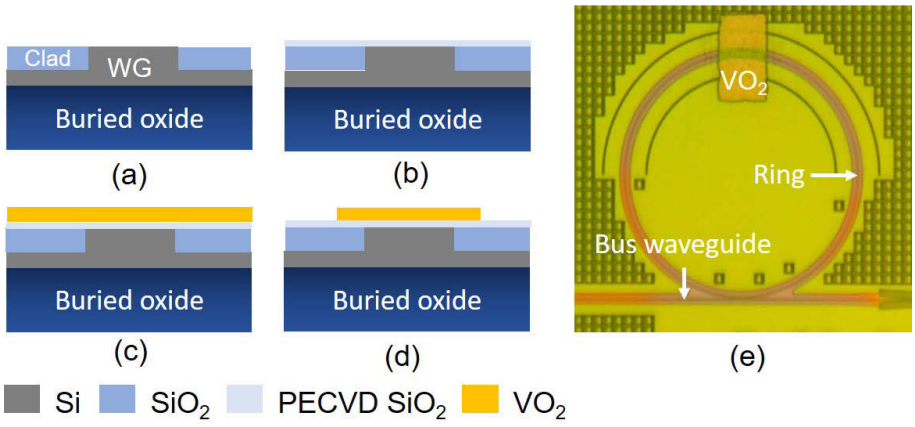

Fig. 4. (a-d) Fabrication process flow of VO_2 modulator, and (e) Microscope image of the ring resonator with VO_2 tab.

3.2. Substrate heating

Figure 4(e) shows the optical microscope image of the fabricated device. Optical characterization of the fabricated device is done using a tunable laser source (1510-1630 nm) and InGaAs photodetector. The light is coupled in and out through focused grating coupler fabricated on the Si device layer of SOI substrate. To perform temperature dependant measurement, a temperature-controlled sample stage was used. All the measurements were performed after the temperature is stabilized at a set temperature.

Figure 5(a) shows temperature-dependent transmission spectrum of a ring resonator with VO_2-patch. The transmission through the device is normalized to reference waveguide to extract the insertion loss. As explained in Section. 2 with increasing in temperature, VO_2 undergoes transition from dielectric to metallic phase. The transition increases loss in the ring cavity resulting in a resonance extinction reduction. In the initial dielectric phase, the ring is observed to be in a critical-coupled regime, the transition to the metallic phase pushes the ring into under-coupled regime reducing the quality factor and extinction of the resonance. The evolution is measured for both heating and cooling cycle which is presented in Fig. 5(b). The loss in the system is calculated from the spectral measurement using the following relation,

$$Loss\ (dB) = \frac{2\pi n_g L}{\lambda_{res} Q_{ring}} \tag{1}$$

where n_g is the group index, L is the geometric path length, λ_{res} is the resonance wavelength, and Q_{ring} is the quality factor of the ring resonator. The temperature-dependent extinction ratio and loss are plotted in Fig. 5(b) and 5(c), respectively. It is apparent that the extinction ratio change is 25 dB and change in loss is around 0.4 dB across the phase transition. Similar to temperature-dependent electrical conductivity measurement, a thermal hysteresis has been observed in extinction ratio and loss during the heating and cooling cycle. Figure 5 shows the hysteresis and transition temperature . We observe a hysteresis of ≈25° extracted from the device spectral response while thin-film hysteresis measured form the electrical resistance and refractive index change (Fig. 2 and 3) shows a narrow hysteresis width of ≈ 12°, which is 13° lower than the hysteresis width measured using a ring resonator. A broader hysteresis width can be attributed to

OSA CONTINUUM

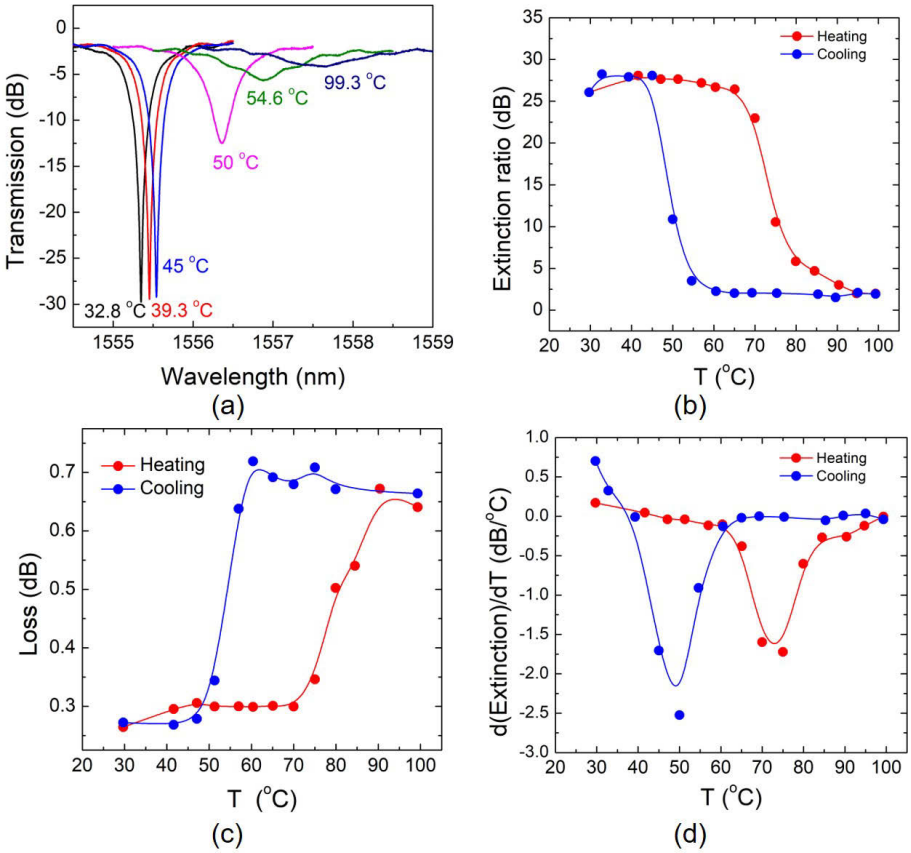

Fig. 5. Summary of spectral characteristics of a substrate heated ring resonator with VO_2 patch. (a) Transmission spectrum of the ring resonator at various temperature, (b) Extinction ratio, (c) Cavity loss, and (d) $d(Extinction)/dT$ during heating and cooling cycle of the substrate. The solid line through the points are provided to guide the eyes.

the thermo-optic interplay between Si and VO_2. Silicon has a positive thermo-optic coefficient $dn/dT = 1.8 \times 10^{-4}/K$. For $T > T_{MIT}$, shift in spectrum due to VO_2 and silicon is opposite in nature. It can be observed in Fig. 5(a) that the spectrum is only red-shifted dominated by silicon layer. In order to negate the substrate effect and probe the effect of VO_2 layer alone, a local heated configuration is necessary, which is presented in the following section.

3.3. Lateral heating

Figure 6(a) and 6(b) shows the schematic of the cross-section and microscope image of a final device with lateral heaters. The lateral micro-strip heater would allow local heating of VO_2. The length of the VO_2 patch is 19 μm long. The heater is designed to be 3 μm wide and 20 μm long placed 5 μm away from the waveguide. Titanium/Platinum (10/90 nm) is used as the heater material stack. The heater stack is deposited using sputter deposition. A similar experimental setup as explained in Section. 3.2 is used while the VO_2 is locally heated by applying a current through the micro-strip heater.

Figure 6(c) shows the transmission spectrum of the micro-ring resonator with increasing heater power. We measure an insertion loss of 1.4 dB across IMT regime, which is one of the lowest reported [18]. The IMT is achieved by locally heating the VO_2 using lateral micro-heaters. As the

OSA CONTINUUM

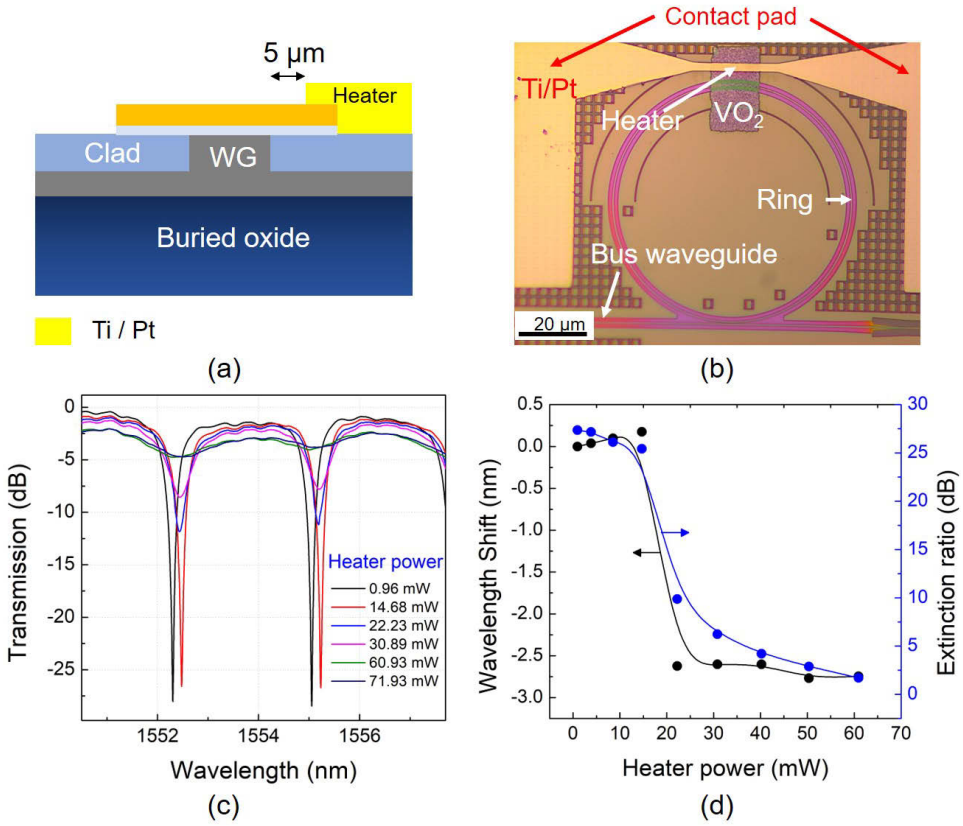

Fig. 6. Summary of spectral characteristics of a ring resonator with a lateral heater. a) Schematic of a device with lateral heaters, b) Microscope image of a ring resonator with VO_2 patch, c) Transmission spectrum of a resonator with increasing heater power, and d) Wavelength shift and extinction ratio evolution with increasing heater power. The solid line through the points are provided to guide the eyes.

temperature increases, the change in refractive index of the material results in a spectral change in the ring response across the phase transition. We observe a blue shift in the spectrum when the heater power exceeds 20 mW accompanied with reduction in extinction ratio. Figure 6(d) shows the extinction ratio and wavelength shift extracted from the transmission spectrum. The change in refractive index in VO_2 can be calculated by using effective index change from Eq. (2) [32], since the equivalent thermo-optic coefficient (TOC) of a waveguide system (dn_{eff}/dT) is a superposition of the TOC of the individual materials, which is given by,

$$\frac{dn_{eff}}{dT} = \sum_i \frac{d(\Gamma_i n_i)}{dT} = \Gamma_{Si}\frac{dn_{Si}}{dT} + \Gamma_{SiO_2}\frac{dn_{SiO_2}}{dT} + \Gamma_{VO_2}\frac{dn_{VO_2}}{dT} \tag{2}$$

Here, Γ_i is the confinement factor in i^{th} material and dn_i/dT is the TOC of the material. A TOC of $1.8 \times 10^{-4}/°C$ is used for Si in the calculation. The confinement factor in silicon and VO_2 is obtained using finite difference modal simulation. Since the refractive index of the VO_2 changes across T_{MIT}, the confinement factor in the waveguide and VO_2 changes. The change in the effective index of the propagating mode in the waveguide, Δn_{eff} is calculated from the spectral shift using Eq. 3 [33].

$$\frac{dn_{eff}}{dT} = \frac{2\pi R\Delta\lambda}{\lambda_0 L} \tag{3}$$

OSA CONTINUUM

where n_{eff} is the effective index of the waveguide, R is the radius of the ring (35 μm), $\Delta\lambda$ is the measured wavelength shift from the spectrum, λ_0 is the centre wavelength of the ring without VO_2, and L is the length of the VO_2 patch (19 μm).

From the spectral characteristics, the ring resonator with dielectric VO_2 in critically coupled regime; high-quality factor and extinction. As the temperature is increased using strip-heater, at lower heater power, we observe a slight red-shift in the spectrum due to thermo-optic shift from Si. However, at the onset of transition, the loss in the cavity increases due to metallic phase of VO_2 that reduces the extinction along with appreciable blue-shift in the spectrum due to reduction in the effective refractive index as shown in Fig. 3. From the measurements, we estimate a refractive index change of 1.2, which agrees well with the literature report [14]. Furthermore, we estimate cavity loss increase from 0.96 dB to 2.79 dB during the insulator to metallic transition, respectively.

3.4. Time domain measurement

The switching behaviour and performance of the device are evaluated using a symmetric Mach-Zehnder Interferometer (MZI). Figure 7(a) shows a microscope image of a symmetric MZI with a 30 μm VO_2 patch on the balanced arms. The phase transition is driven by a micro-strip heater as mentioned in the previous section 3.3. Figure 7(b) shows the transmission spectrum of the MZI at various heater power. For heater powers >126 mW, the phase transition from insulating-to-metallic state starts. Figure 7(c) shows the insertion loss at various heater power. A maximum loss of 25 dB is achieved at a heater power of 168 mW.

The dynamic response of the device is characterized by driving both the arms using a 10 KHz square waveform. Though a maximum transmission extinction of 25 dB is achieved through DC drive, the maximum speed of switching depends on the operating point of the material. Furthermore, the size of the VO_2 patch also plays a crucial role in switching speed. In order to obtain the best performance of the device, it is biased near the dielectric phase, and the amplitude of the voltage swing is varied from 1 V_{pp} to 4 V_{pp}. Figure 7(d) shows the modulated optical output for a fixed heater power (DC) with variable voltage swing (AC).

The raising edge represents MIT, and falling edge indicates IMT. With an increase in the drive voltage, we observe an increase in the modulation extinction until 3.5 V_{pp} and falls beyond. Furthermore, beyond 3 V_{pp} the insertion loss increases. The change in the modulation extinction and insertion loss can be attributed to the phase transition due to the drive voltage swing. At lower drive voltages the transition is not fully metallic resulting in lower modulation and insertion loss. However, at higher drive voltages, the transition is pushed deep into metallic resulting in higher insertion loss and transition as well. The transition characteristics also affect the phase transition time as well. With increasing drive voltage, the rise time and fall time increases from 2.15 μs to 13.2 μs and 1.39 μs to 7.49 μs, respectively. It can also be seen that IMT is quicker than MIT transition. The experiment is repeated by fixing the voltage swing of 1.5 V_{pp}, and the bias voltage is varied between 1 V and 2.5 V. For a particular bias voltage, the material's phase is fixed and the time constants related to each bias point is calculated. Figure 7(e) shows the modulated optical output for fixed voltage swing and variable heater power. It can be seen that as the bias voltage increases, the insertion loss of the device increases. After the phase transition (DC>2 V) the insertion loss increases and the optical modulation reduces which clearly shows that bias point has to be chosen near the dielectric phase. Considering the metrics of insertion loss and optical modulation, bias voltage of 1.5 V is the optimum operation point and the obtained rise time and fall time are 4.06 μs and 2.92 μs, respectively.

The optimal operating point depends on various factors such as material quality, hysteresis width, VO_2 patch dimensions and heater efficiency. However, in this work, we have demonstrated a schema to identify optimal operating point to achieve desired performance from a phase-change material based optical switch.

OSA CONTINUUM

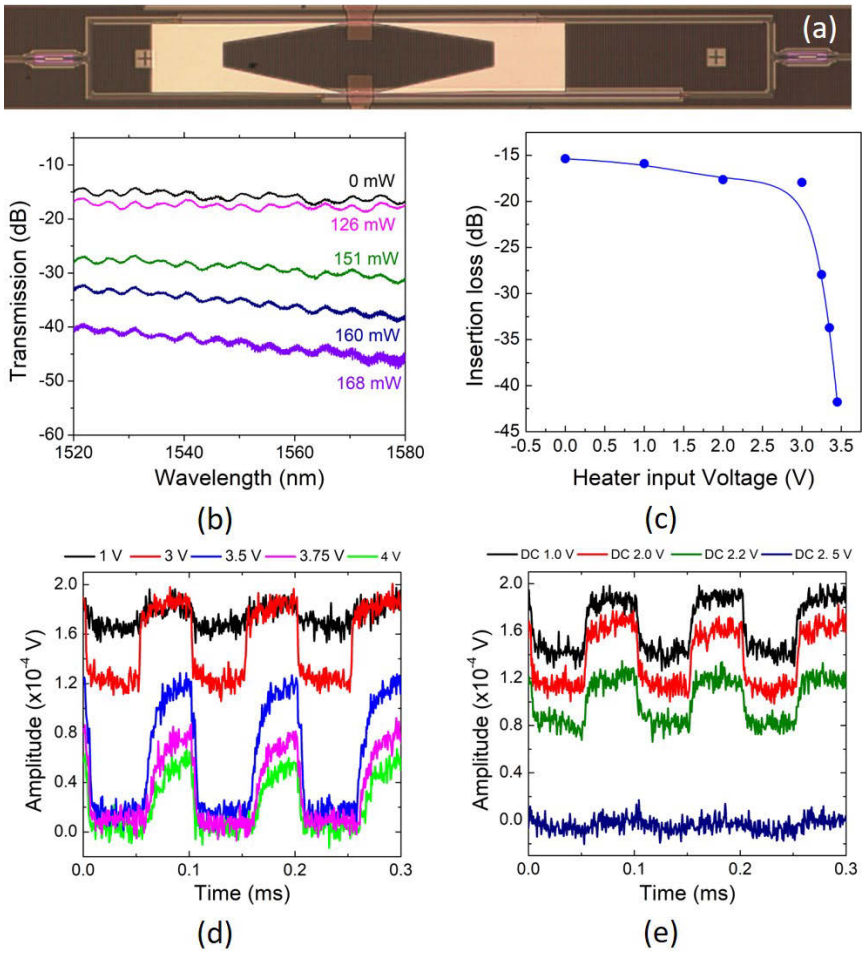

Fig. 7. (a) Microscope image of the Mach-Zehnder interferometer with VO_2 tabs in both the arms, (b) Transmission spectrum of the symmetric Mach-Zehnder interferometer with varying heater power, (c) Insertion loss of the device with varying heater power, and Time domain measurement of the VO_2 based optical modulator with (d) fixed heater power and variable voltage swing and (e) fixed voltage swing and variable heater power. The solid line through the points are provided to guide the eyes.

4. Conclusion

We presented an electrical and optical phase transition of PLD deposited VO_2 film on SOI. We demonstrated complete phase change behaviour of VO_2 and utilized it as an optical switch. We have achieved a maximum transmission extinction of 25 dB. We also measured and verified the refractive index change due to the phase transition. By using a micro-strip heater we demonstrated a maximum transmission extinction of 25 dB with an insertion loss 1.4 dB. We also analyzed the switching performance of an MZI-based device by obtaining the optimum heater power and the voltage swing. We presented a procedure to identify a suitable operating point to achieve maximum switching speed with maximum extinction and minimum insertion loss. We report a maximum switching speed of 118 kHz, which can be improved by reducing the size the VO_2 interaction length, however, with a trade-off of achievable modulation extinction.

OSA CONTINUUM

Funding

Ministry of Electronics and Information technology; Ministry of Human Resource Development; Nano Mission Council, Department of Science and Technology.

Acknowledgment

V.J. wish to thank the facility technologists of National Nano fabrication Centre(NNfC) and Micro and Nano Characterization facility (MNCf), Centre for Nano Science and Engineering, Indian Institute of Science, India for their support in fabrication and characterization. V.J. acknowledges Ministry of Electronics and Information Technology (MeitY), Govt. of India for the student fellowship and S.K.S acknowledges MeitY for the faculty fellowship.

Disclosures

The authors declare no conflicts of interest.

References

1. K. J. Miller, R. F. Haglund, and S. M. Weiss, "Optical phase change materials in integrated silicon photonic devices," Opt. Mater. Express **8**(8), 2415–2429 (2018).
2. K. T. P. Lim, H. Liu, Y. Liu, and J. K. W. Yang, "Broadband transparent optical phase change materials for high-performance nonvolatile photonics," Nat. Commun. **10**(1), 25 (2019).
3. C. Ko and S. Ramanathan, "Dispersive capacitance and conductance across the phase transition boundary in metal-vanadium oxide-silicon devices," J. Appl. Phys. **106**(3), 034101 (2009).
4. J. D. Ryckman, V. Diez-Blanco, J. Nag, R. E. Marvel, B. Choi, R. F. Haglund, and S. M. Weiss, "Photothermal optical modulation of ultra-compact hybrid Si-VO_2 ring resonators," Opt. Express **20**(12), 13215–13225 (2012).
5. A. Cavalleri, C. Tóth, C. W. Siders, J. Squier, F. Ráksi, P. Forget, and J. Kieffer, "Femtosecond structural dynamics in VO_2 during an ultrafast solid-solid phase transition," Phys. Rev. Lett. **87**(23), 237401 (2001).
6. A. Cavalleri, T. Dekorsy, H. H. Chong, J.-C. Kieffer, and R. W. Schoenlein, "Evidence for a structurally-driven insulator-to-metal transition in VO_2: A view from the ultrafast timescale," Phys. Rev. B **70**(16), 161102 (2004).
7. M. F. Becker, A. B. Buckman, R. M. Walser, T. Lépine, P. Georges, and A. Brun, "Femtosecond laser excitation of the semiconductor-metal phase transition in VO_2," Appl. Phys. Lett. **65**(12), 1507–1509 (1994).
8. J. D. Ryckman, K. A. Hallman, R. E. Marvel, R. F. Haglund, and S. M. Weiss, "Ultra-compact silicon photonic devices reconfigured by an optically induced semiconductor-to-metal transition," Opt. Express **21**(9), 10753–10763 (2013).
9. P. Boriskov, A. Velichko, A. Pergament, G. Stefanovich, and D. Stefanovich, "The effect of electric field on metal-insulator phase transition in vanadium dioxide," Tech. Phys. Lett. **28**(5), 406–408 (2002).
10. B. Wu, A. Zimmers, H. Aubin, R. Ghosh, Y. Liu, and R. Lopez, "Electric-field-driven phase transition in vanadium dioxide," Phys. Rev. B **84**(24), 241410 (2011).
11. Y. Zhou, X. Chen, C. Ko, Z. Yang, C. Mouli, and S. Ramanathan, "Voltage-triggered ultrafast phase transition in vanadium dioxide switches," IEEE Electron Device Lett. **34**(2), 220–222 (2013).
12. J. K. Kana, J. Ndjaka, G. Vignaud, A. Gibaud, and M. Maaza, "Thermally tunable optical constants of vanadium dioxide thin films measured by spectroscopic ellipsometry," Opt. Commun. **284**(3), 807–812 (2011).
13. J. Sun and G. K. Pribil, "Analyzing optical properties of thin vanadium oxide films through semiconductor-to-metal phase transition using spectroscopic ellipsometry," Appl. Surf. Sci. **421**, 819–823 (2017).
14. R. M. Briggs, I. M. Pryce, and H. A. Atwater, "Compact silicon photonic waveguide modulator based on the vanadium dioxide metal-insulator phase transition," Opt. Express **18**(11), 11192–11201 (2010).
15. K. J. Miller, K. A. Hallman, R. F. Haglund, and S. M. Weiss, "Silicon waveguide optical switch with embedded phase change material," Opt. Express **25**(22), 26527–26536 (2017).
16. I. Olivares, L. Sanchez, J. Parra, R. Larrea, A. Griol, M. Menghini, P. Homm, L.-W. Jang, B. Van Bilzen, J. W. Seo, J.-P. Locquet, and P. Sanchis, "Optical switching in hybrid VO_2/Si waveguides thermally triggered by lateral microheaters," Opt. Express **26**(10), 12387–12395 (2018).
17. P. Markov, K. Appavoo, R. F. Haglund, and S. M. Weiss, "Hybrid Si-VO_2-Au optical modulator based on near-field plasmonic coupling," Opt. Express **23**(5), 6878–6887 (2015).
18. A. Joushaghani, J. Jeong, S. Paradis, D. Alain, J. S. Aitchison, and J. K. Poon, "Wavelength-size hybrid Si-VO_2 waveguide electroabsorption optical switches and photodetectors," Opt. Express **23**(3), 3657–3668 (2015).
19. W. H. Pernice and H. Bhaskaran, "Photonic non-volatile memories using phase change materials," Appl. Phys. Lett. **101**(17), 171101 (2012).
20. C. Ríos, M. Stegmaier, P. Hosseini, D. Wang, T. Scherer, C. D. Wright, H. Bhaskaran, and W. H. Pernice, "Integrated all-photonic non-volatile multi-level memory," Nat. Photonics **9**(11), 725–732 (2015).

OSA CONTINUUM

21. M. Currie, M. A. Mastro, and V. D. Wheeler, "Characterizing the tunable refractive index of vanadium dioxide," Opt. Mater. Express **7**(5), 1697–1707 (2017).
22. M. Wuttig, H. Bhaskaran, and T. Taubner, "Phase-change materials for non-volatile photonic applications," Nat. Photonics **11**(8), 465–476 (2017).
23. S. B. Lee, K. Kim, J. S. Oh, B. Kahng, and J. S. Lee, "Origin of variation in switching voltages in threshold-switching phenomena of VO_2 thin films," Appl. Phys. Lett. **102**(6), 063501 (2013).
24. J. Jeong, N. Aetukuri, T. Graf, T. D. Schladt, M. G. Samant, and S. S. Parkin, "Suppression of metal-insulator transition in VO_2 by electric field–induced oxygen vacancy formation," Science **339**(6126), 1402–1405 (2013).
25. S. Lee, T. L. Meyer, S. Park, T. Egami, and H. N. Lee, "Growth control of the oxidation state in vanadium oxide thin films," Appl. Phys. Lett. **105**(22), 223515 (2014).
26. T. Maruyama and Y. Ikuta, "Vanadium dioxide thin films prepared by chemical vapour deposition from vanadium (III) acetylacetonate," J. Mater. Sci. **28**(18), 5073–5078 (1993).
27. S. N. Gupta, A. Pal, D. Muthu, P. A. Kumar, and A. Sood, "Metallic monoclinic phase in VO_2 induced by electrochemical gating: In situ raman study," Eur. Phys. Lett. **115**(1), 17001 (2016).
28. R. Bharathi, R. Naorem, and A. Umarji, "Metal–insulator transition characteristics of vanadium dioxide thin films synthesized by ultrasonic nebulized spray pyrolysis of an aqueous combustion mixture," J. Phys. D: Appl. Phys. **48**(30), 305103 (2015).
29. B. Rajeswaran and A. Umarji, "Phase evolution and infrared transmittance in monophasic VO_2 synthesized by a rapid non-equilibrium process," Mater. Chem. Phys. **190**, 219–229 (2017).
30. B. Rajeswaran, J. K. Pradhan, S. Anantha Ramakrishna, and A. M. Umarji, "Thermochromic VO_2 thin films on ito-coated glass substrates for broadband high absorption at infra-red frequencies," J. Appl. Phys. **122**(16), 163107 (2017).
31. Europractice: MPW, "iSiPP25G," https://europractice-ic.com/mpw-prototyping/siphotonics/imec/.
32. S. Feng, K. Shang, J. T. Bovington, R. Wu, B. Guan, K.-T. Cheng, J. E. Bowers, and S. B. Yoo, "Athermal silicon ring resonators clad with titanium dioxide for 1.3 μm wavelength operation," Opt. Express **23**(20), 25653–25660 (2015).
33. W. Bogaerts, P. De Heyn, T. Van Vaerenbergh, K. De Vos, S. Kumar Selvaraja, T. Claes, P. Dumon, P. Bienstman, D. Van Thourhout, and R. Baets, "Silicon microring resonators," Laser Photonics Rev. **6**(1), 47–73 (2012).